IEEE Access
Multidisciplinary ⋮ Rapid Review ⋮ Open Access Journal

Received 6 October 2022, accepted 8 November 2022, date of publication 18 November 2022, date of current version 10 February 2023.

Digital Object Identifier 10.1109/ACCESS.2022.3223385

RESEARCH ARTICLE

Robust Finite Control Set Model Predictive Current Control for Induction Motor Using Deadbeat Approach in Stationary Frame

THIAGO BALDIM DOS SANTOS[1], IGOR OLIANI[1], RAFAEL FIGUEIREDO[1], DANIEL ALBIEIRO[2], ADEMIR PELIZARI[1], AND ALFEU J. SGUAREZI FILHO[1], (Senior Member, IEEE)

[1]CECS Department, Federal University of ABC, Santo André 09210-580, Brazil
[2]School of Agricultural Engineering, University of Campinas, FEAGRI, Campus Zeferino Vaz, Campinas, São Paulo 13083-875, Brazil

Corresponding author: Alfeu J. Sguarezi Filho (alfeu.sguarezi@ufabc.edu.br)

This work was supported in part by the Research and Development Foundation—Fundep Rota 2030/Linha V process under Grant 27192.03.01/2020.13-00, and in part by the National Council for Scientific and Technological Development [Conselho Nacional de Desenvolvimento Científico e Tecnológico (CNPq)] under Grant 405757/2018-2 and Grant 407867/2022-8.

ABSTRACT The model predictive control increased its prominence in the field of induction machine drives. However, the performance of this strategy depends on the accuracy of the machine model parameters. In order to overcome this deficiency, this paper proposes a robust model predictive current control employing indirect field-oriented control in stationary reference frame using the stator current and the rotor flux vectors as state and stator voltage vector as the input. The control algorithm combines the classical model predictive control with the deadbeat approach in order to calculate the applied stator voltage vector in two components: one element considers the stator current reference, and another employs the disturbances caused due to the parameter errors, which allows to compensate the parameter mismatches in the plant model. The minimized cost function employs the predicted stator voltage vector to select the voltage vector to be applied to the stator terminals of the motor. The control method performance was verified using an experimental test bench analyzing the system steady-state and dynamic actions. In this way, the results corroborate the proposed controller robustness against parametric variations.

INDEX TERMS Induction motor, model predictive control, robust predictive control, current control, parameter variations, deatbeat, indirect field oriented control.

I. INTRODUCTION

The induction motor (IM) has been widely used in applications that demand high torque control accuracy over a wide speed range such as in electric vehicles [1], [2], [3], [4], [5]. Considering the control strategies for IM, one solution that has recently been used is the model predictive control (MPC) due to its high flexibility and simplicity [6], [7]. The basic idea of MPC is to use a model of a plant to predict the behavior of system variables within a time horizon. In this way, the minimization of a cost function using the idealized and the predicted behavior, an optimized control performance can be obtained selecting the control input to the system [8], [9]. However, the classical MPC employs the model of the IM to design the controllers. So, it can degrade the performance of the controller due to the parameter errors.

Recently, some MPC strategies have been proposed in order to increase the robustness against parameters mismatch of the machines as presented in [10], [11], [12], and [13]. In [14], the ordinary MPC employs the nonlinear model considering the taylor representation of IM for each equilibrium point. A predictive torque control for IM employing a combined integral sliding mode observer and an adaptive Luenberger observer was presented in [15].

The work [16] proposes a model-free predictive current control (MFPCC) based on the ultra-local model. The whole

The associate editor coordinating the review of this manuscript and approving it for publication was Jiefeng Hu.

controller only needs the input and output data without the need for the motor parameters. In [17], a model-free control is also proposed and the control signal is determined by the sampled current and the current error. In [18] and [19], linear extended state observers are employed to this task. The robust MPC considering a generalized proportional-integral observer is presented in [20]. The reported results are satisfactory during the IM parameter errors.

In [21], it is proposed a robust deadbeat predictive current control (DPCC), which employs the error between the measured currents and the predicted currents to compensate the influence of machine parameter mismatches. This method presents a good robustness against parameter mismatches.

Aiming to decrease the error of the stator current prediction, [22] and [23] employ the Luenberger observer to achieve this goal. The robust deadbeat-based current control presented by [22] has satisfactory dynamic performance and strong robustness in the experimental tests compared to PI current control and traditional deadbeat. The experimental results of the MPC strategy proposed by [23] have superior performance against the traditional MPC current control.

This paper proposes a robust finite control set model predictive current control for IM in stationary reference frame using the stator current and the rotor flux vectors as state and stator voltage vector as the input variables. The proposal employs indirect field-oriented control (IFOC) and presents its structural robustness properties [24]. In this case, the proposed solution computes two stator voltage vectors in which one predicts the voltage vector considering the classical MPC and another stator voltage vector element considering the deadbeat approach to compensate the parameter errors of the IM. Hence, the minimized cost function considering the cited voltage elements selects the stator voltage vector to be applied to the stator terminals of the IM. The results endorse the performance of the proposed robust model predictive current control in stationary frame for IM in normal operation, during the presence of the parameter errors and against the classical predictive current control.

II. ROBUST FINITE CONTROL SET MODEL PREDICTIVE CURRENT CONTROL FOR IM

The proposed robust finite control set model predictive current control of IM employs IFOC. In this way, the proposal predicts the future actions of the stator voltage vector of IM considering the parameter mismatches, selecting the voltage vector to be applied to the stator of the IM considering the minimization of the cost function. The mentioned cost function was computed by using the predicted and the reference voltage vectors.

A. INDUCTION MOTOR MODELLING

The model of IM can be expressed using the vector notation and it can be represented in the stationary frame according to [25]:

$$\vec{i}_{\alpha\beta s} + \tau_\sigma \frac{d\vec{i}_{\alpha\beta s}}{dt} = \frac{k_r}{R_\sigma}\left(\frac{1}{\tau_r} - jp\omega_{mec}\right)\vec{\psi}_{\alpha\beta r} + \frac{\vec{v}_{\alpha\beta s}}{R_\sigma} \quad (1)$$

$$\vec{\psi}_{\alpha\beta r} + \tau_r \frac{d\vec{\psi}_{\alpha\beta r}}{dt} = jp\omega_{mec}\tau_r\vec{\psi}_{\alpha\beta r} + L_m\vec{i}_{\alpha\beta s} \quad (2)$$

$$T_{em} = \frac{3}{2}pIm\{\vec{\psi}^*_{\alpha\beta s}\vec{i}_{\alpha\beta s}\} \quad (3)$$

$$J_m\frac{d\omega_{mec}}{dt} = T_{em} - T_{load} \quad (4)$$

where $\tau_r = L_r/R_r$; $\sigma = 1 - (L_m^2/L_sL_r)$; $k_r = L_m/L_r$; $R_\sigma = R_s + R_r(L_m^2/L_r^2)$; $\tau_\sigma = \sigma L_s/R_\sigma$. L_r and L_s are the self inductance of the rotor and stator and L_m corresponds to the mutual inductance. R_r and R_s are the rotor, stator resistances. J_m is the total inertia, T_{load} is the load torque, p is the number of pole pairs and ω_{mec} is the rotor mechanical speed. The vectors $\vec{i}_{\alpha\beta s} = i_\alpha + ji_\beta$; $\vec{v}_{\alpha\beta s} = v_\alpha + jv_\beta$ and $\vec{\psi}_{\alpha\beta r} = \psi_{\alpha r} + j\psi_{\beta r}$ are from the stator current, the stator voltage, and the rotor magnetic flux, respectively. The symbol "$*$" expresses the conjugate of the complex number.

B. ROBUST FINITE CONTROL SET CURRENT CONTROL

This proposal of predictive current control considers the errors in the estimation of the machine parameters in the controller for the prediction of the stator voltage vector (5). The predicted voltage vector $\vec{v}^{\,p}_{\alpha\beta s}(k)$ is composed of two components: one for the voltage calculated considering the stator current reference $\vec{v}_{ff}(k)$, and another for the voltage that takes into account the parametric errors of the IM ($\vec{v}_{fb}$). The parametric mismatches are modeled around variations in stator currents.

$$\vec{v}^{\,p}_{\alpha\beta s}(k) = \vec{v}_{ff}(k) + \vec{v}_{fb}(k) \quad (5)$$

The selection of the voltage vector to be applied to the stator terminals is performed by using the minimization of the cost function g (6), in which it is limited to the voltage levels that can be applied by the inverter ($\vec{v}^{\,ref}_{\alpha\beta s}$).

$$g = |\vec{v}^{\,ref}_{\alpha\beta s} - \vec{v}^{\,p}_{\alpha\beta s}(k)| \quad (6)$$

This minimization ensures that the behavior of the controlled variable reaches the reference signal.

The presented control method uses a two-level voltage source inverter (VSI) which enable the application of eight voltage vectors as presented in Table 1.

TABLE 1. Switching states and voltage vectors of VSI.

Vector	S_1	S_2	S_3	$\vec{v}^{\,x}_{\alpha\beta s}$
$\vec{v}^{\,0}_{\alpha\beta s}$	0	0	0	$0\,V_{cc}$
$\vec{v}^{\,1}_{\alpha\beta s}$	1	0	0	$\frac{2}{3}V_{cc}$
$\vec{v}^{\,2}_{\alpha\beta s}$	1	1	0	$(\frac{1}{3} + j\frac{\sqrt{3}}{3})V_{cc}$
$\vec{v}^{\,3}_{\alpha\beta s}$	0	1	0	$(-\frac{1}{3} + j\frac{\sqrt{3}}{3})V_{cc}$
$\vec{v}^{\,4}_{\alpha\beta s}$	0	1	1	$-\frac{2}{3}V_{cc}$
$\vec{v}^{\,5}_{\alpha\beta s}$	0	0	1	$(-\frac{1}{3} - j\frac{\sqrt{3}}{3})V_{cc}$
$\vec{v}^{\,6}_{\alpha\beta s}$	1	0	1	$(\frac{1}{3} - j\frac{\sqrt{3}}{3})V_{cc}$
$\vec{v}^{\,7}_{\alpha\beta s}$	1	1	1	$0\,V_{cc}$

The vector $\vec{v}^{\,x}_{\alpha\beta s}$ is expressed as:

$$\vec{v}^{\,x}_{\alpha\beta s} = \frac{2}{3}(S_1 + aS_2 + a^2S_3)V_{dc} \quad (7)$$

where S_i represents the switching state of each i arm of the inverter, $a = e^{j\frac{2\pi}{3}}$ and V_{dc} is the dc-link voltage.

The relationship between the stator current, the rotor flux and the voltage vectors is shown in (1). Hence, it can be employed to represent $\vec{v}_{ff}(k)$. The starting point for calculating $\vec{v}_{ff}(k)$ is the discretization of (1) using the Euler's method for a sampling time T_s [11], [26]. In this way, the discretization of (1) is expressed by:

$$\frac{\vec{v}_{\alpha\beta s}(k)}{R_\sigma} = \tau_\sigma \frac{\Delta\vec{i}_{\alpha\beta s}(k)}{T_s} + \vec{i}_{\alpha\beta s}(k) - \frac{k_r}{R_\sigma}\left(\frac{1}{\tau_r} - jp\omega_{mec}\right)\vec{\psi}_{\alpha\beta r}(k) \quad (8)$$

where $\Delta\vec{i}_{\alpha\beta s}(k) = \vec{i}_{\alpha\beta s}(k+1) - \vec{i}_{\alpha\beta s}(k)$ for the instant k.

The calculation of $\vec{v}_{ff}(k)$ can be performed using (8). In this case, $\Delta\vec{i}_{\alpha\beta s}(k) = \vec{i}^{\,ref}_{\alpha\beta s} - \vec{i}_{\alpha\beta s}(k)$, in which $\vec{i}_{\alpha\beta s}(k+1) = \vec{i}^{\,ref}_{\alpha\beta s}$ is the stator current vector reference. So, it can be expressed as:

$$\vec{v}_{ff}(k) = R_\sigma\left(\tau_\sigma \frac{\Delta\vec{i}_{\alpha\beta s}(k)}{T_s} + \vec{i}_{\alpha\beta s}(k)\right) - k_r\left(\frac{1}{\tau_r} - jp\omega_{mec}\right)\vec{\psi}_{\alpha\beta r}(k) \quad (9)$$

The calculation of $\vec{v}_{fb}(k)$ can be performed using (8) delayed one sampling time as presented in (10).

$$\frac{\vec{v}_{\alpha\beta s}(k-1)}{R_\sigma} = \tau_\sigma \frac{\Delta\vec{i}_{\alpha\beta s}(k-1)}{T_s} + \vec{i}_{\alpha\beta s}(k-1) - \frac{k_r}{R_\sigma}\left(\frac{1}{\tau_r} - jp\omega_{mec}\right)\vec{\psi}_{\alpha\beta r}(k-1) \quad (10)$$

where $\Delta\vec{i}_{\alpha\beta s}(k-1) = \vec{i}_{\alpha\beta s}(k) - \vec{i}_{\alpha\beta s}(k-1)$ for the instant $(k-1)$.

Subtracting (10) to (8) for a stator current increment at the instant k, considering $\Delta\vec{i}_{\alpha\beta s}(k) = 0$ and the dynamic action of the rotor flux is slower than the stator flux, i.e., $\vec{\psi}_{\alpha\beta r}(k) \cong \vec{\psi}_{\alpha\beta r}(k-1)$. The result can be observed in (11).

$$\frac{\vec{v}_{\alpha\beta s}(k) - \vec{v}_{\alpha\beta s}(k-1)}{R_\sigma} = -\frac{\tau_\sigma \Delta\vec{i}_{\alpha\beta s}(k-1)}{T_s} + \Delta\vec{i}_{\alpha\beta s}(k-1) \quad (11)$$

The assumption ($\Delta\vec{i}_{\alpha\beta s}(k) = 0$) is performed to ensure that there is no increment due to parameter mismatches of the IM [11], [27].

The (11) can be rearranged in the form of:

$$\vec{v}_{\alpha\beta s}(k) - \vec{v}_{\alpha\beta s}(k-1) = R_\sigma\left(1 - \frac{\tau_\sigma}{T_s}\right)\Delta\vec{i}_{\alpha\beta s}(k-1) \quad (12)$$

Equation (12) permits to calculate the stator voltage vector increment when there is increment in stator current vector due to the parameter mismatch of the plant. In this case, the idea behind the definition of the component $\vec{v}_{fb}$ is to express it as a function of the variation of the stator current vector due to the errors associated with the plant parameters. So, $\vec{v}_{fb}$ using (12) is defined in (13).

$$\vec{v}_{fb} = -G\Delta\vec{i}_{\alpha\beta s}(k-1) \quad (13)$$

where G represents the gain defined as:

$$G = -R_\sigma\left(1 - \frac{\tau_\sigma}{T_s}\right) \quad (14)$$

Which permits the calculation of $\vec{v}_{fb}(k)$ and it can be expressed as:

$$\vec{v}_{fb}(k) = -R_\sigma\left(1 - \frac{\tau_\sigma}{T_s}\right)\Delta\vec{i}_{\alpha\beta s}(k-1) \quad (15)$$

The calculation of $\vec{v}^{\,p}_{\alpha\beta s}(k)$ can be described in (5); the voltage vectors $\vec{v}_{ff}(k)$ and $\vec{v}_{fb}(k)$ are obtained employing the Eqs. (9) and (15), respectively. Therefore, the minimized cost function in (6) is computed using the predicted values of $\vec{v}^{\,p}_{\alpha\beta s}(k)$ and the eight voltage levels of the inverter. Hence, the proposed solution permits to control the stator current vector of the IM.

Figure 1 shows the block diagram representation for the implemented Robust Model Predictive Current Control for IM. The current references i^{ref}_{ds} and i^{ref}_{qs} are computed considering the rotor flux magnitude and the torque signals, as presented in (16) and (17), considering the use of rotor field oriented control. After performing transformation of i^{ref}_{ds} and i^{ref}_{qs} from the synchronous reference frame to the stationary reference frame using the rotor flux vector position, $i^{ref}_{\alpha s}$ and $i^{ref}_{\beta s}$ are obtained.

$$i^{ref}_{ds} = \frac{|\vec{\psi}_{\alpha\beta r}|^{ref}}{L_m} \quad (16)$$

$$i^{ref}_{qs} = \frac{3}{2}\frac{L_r}{L_m^2}\frac{T^{ref}_{em}}{i^{ref}_{ds}} \quad (17)$$

The variables presented in Fig. 1, w_s and w_{ele} represent the slip speed and the electrical synchronous speed, respectively.

III. EXPERIMENTAL RESULTS

The presented control method was implemented on an experimental test bench shown in Fig. 2. The test bench is composed by an 1.1 kW squirrel-cage IM driven by a two?level voltage source inverter with a dc-link voltage controlled by a 3 kVA variac. The load torque applied on the motor shaft is done by an eddy current brake. The control system is composed by Texas Instruments development board LAUNCHXL-F28379D with TMS320F28379D microprocessor incorporated, using auxiliary circuits built in the laboratory for signal conditioning. A 3600 pulse per revolution incremental encoder measures the rotor position.

The IM parameters are: nominal electromagnetic torque is 6.18 N·m; nominal speed is 1700 rpm; nominal frequency is 60 Hz; *pole pairs* $= 2$; $R_s = 7.1\ \Omega$; $R_r = 3.98\ \Omega$; $L_s = 545$ mH; $L_r = 545$ mH and $L_m = 526$ mH. The inverter was operated with constant dc-link voltage, so $V_{dc} = 412$ V. The control algorithm runs at a sampling frequency of 20 kHz and uses one-step prediction horizon. The PI controller used in speed control loop was tuned in a process of trial and error.

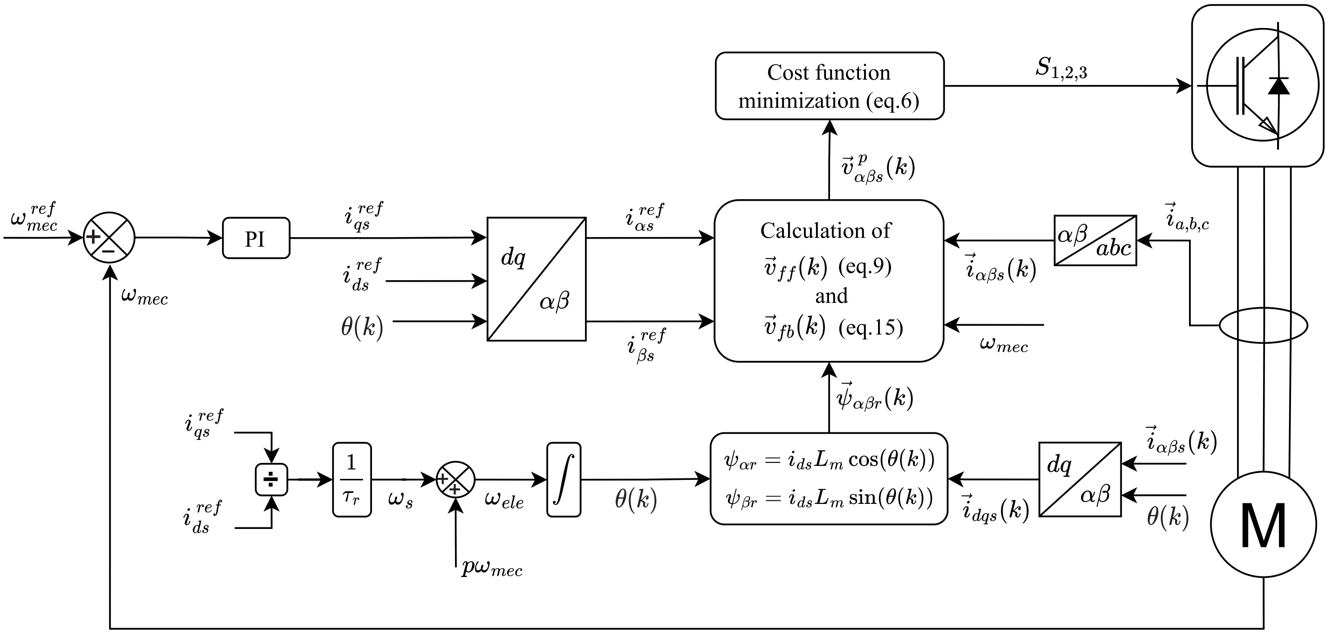

FIGURE 1. Block diagram of proposed robust predictive current control for IM.

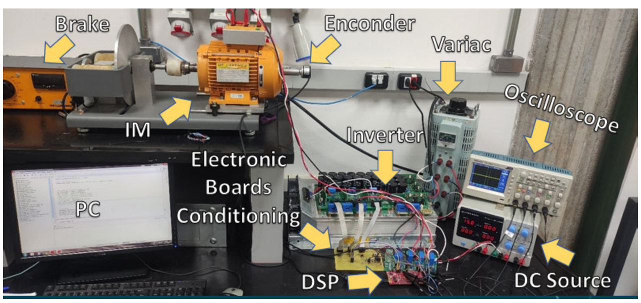

FIGURE 2. Experimental setup.

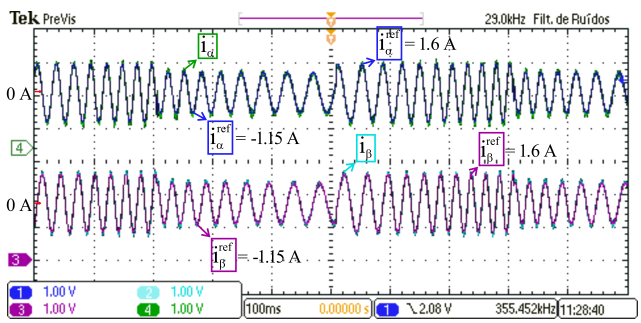

FIGURE 3. Stator current components waveforms of the proposed control method to $|\vec{i}_{s\alpha\beta}|$ steps.

A. DYNAMIC BEHAVIOR WITHOUT SPEED CONTROL LOOP

The first test was conducted with no load to verify the performance of the proposed control method using the $i_{\alpha s}$ and $i_{s\beta}$ as control commands (Fig. 3). The signals of $i_{\alpha s}^{ref}$ and $i_{\beta s}^{ref}$ were generated after the conversion of i_{ds}^{ref} and i_{qs}^{ref} components to the stationary frame as previously explained. A reference step from 1.14 A to 1.62 A was applied for both components.

The results for $\vec{i}_{\alpha\beta s}$ components allow us to observe that the elements of the stator currents reaches the references. It is possible to observe in steady state periods that as rotor speed raises the current frequency also increases. In the interval of 0.65 s to 0.775 s the mean absolute error (MAE) for $i_{\alpha s}$ is 0.074 A and for $i_{\beta s}$ is 0.058 A. The values of root mean square error (RMSE) are 0.09 A for alpha component and 0.072 A for beta component of the stator current. The calculated current total harmonic distortion (THD) registered for the currents is 7.48%.

The action of the elements is depicted in details in Fig. 4(a) and (b). The equivalent step response of the stator current vector magnitude $|\vec{i}_{s\alpha\beta}|$ is plotted in Fig. 4(c) and its setting time is 0.5 ms with no overshoot. After the settling time period, the peak to peak ripple for the measured values was estimated in 0.1858 A. The MAE is 0.0285 A and the mean relative error (MRE) is 1.76%.

B. DYNAMIC BEHAVIOR WITH SPEED CONTROL LOOP

The performance of the control method with speed control loop was evaluated by two tests. In the first one the speed range control was evaluated varying the rotor speed from −570 rpm to 570 rpm with no load applied on the motor shaft. The signals of speed, torque and one phase of stator current measured during the test are depicted in Fig. 6. The proportional and integral gains of the PI controller were set at 0.3 and 0.1, respectively.

The settling time is 80 ms for the reversing process in which the maximum torque applied was limited to 6 N·m and it is nearly its nominal value. After the setting time, the MAE

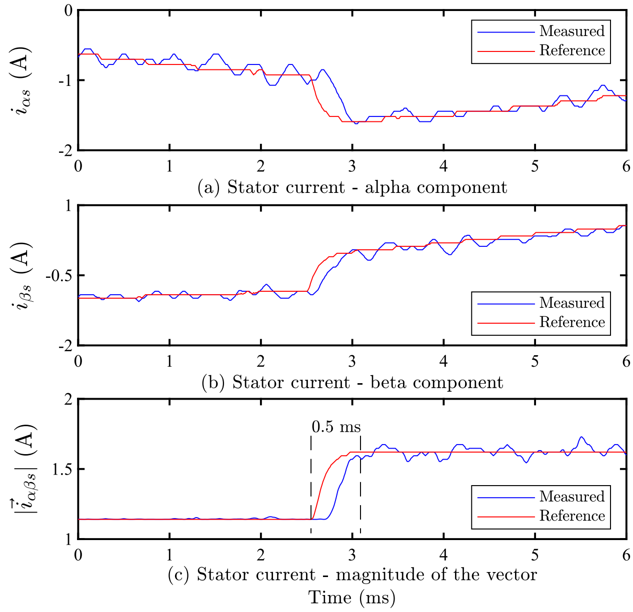

FIGURE 4. **Zoom in stator current components waveforms and $|\vec{i}_{s\alpha\beta}|$ step response.**

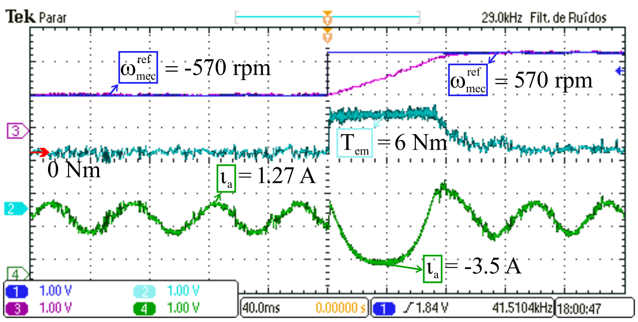

FIGURE 5. **Speed, torque and stator phase current waveforms in a partial-speed reversal maneuver.**

is 9.4 rpm and the MRE is 1.7%. The control system followed the speed reference and presented low torque ripples. The stator current has an amplitude near 1.3 A in steady-state and, during the reversion of the speed, a peak of −3.5 A during the test.

Another test was carried out considering the rated mechanical speed. In this case, it was applied a speed step from −1700 rpm to 1700 rpm with no load on the motor shaft. The speed, torque and stator phase current measured during the test are presented in Fig. 6. The proportional and integral gains of the PI controller were set at 0.1 and 0.3, respectively. In this test, the setting time is 270 ms, the MAE is 35.8 rpm, and the MRE is 2.1%.

In a third test, a load torque (T_{load} = 4.6 N·m) is applied to the motor shaft while the speed is maintained constant and it is depicted in Fig. 7. The reference speed was set at 570 rpm and the eddy current brake was switched on for a short period of time changing the load torque from 0.3 N·m to 4.6 N·m until it is switched off again. The proportional and integral

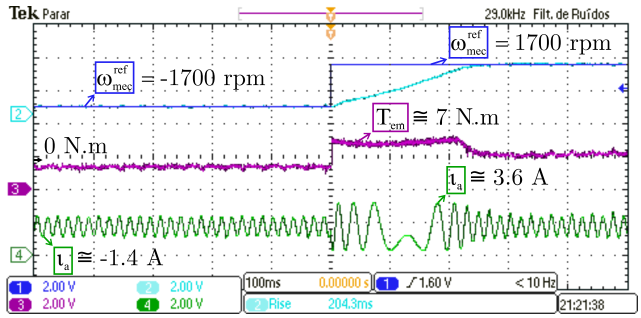

FIGURE 6. **Speed, torque and stator phase current waveforms in a complete-speed reversal maneuver.**

gains of the PI controller were set at 0.1 and 0.3, respectively. Thus, the electromagnetic torque reference calculated by the PI controller could be properly attended for the torque reference as long as the rotor speed reached its reference.

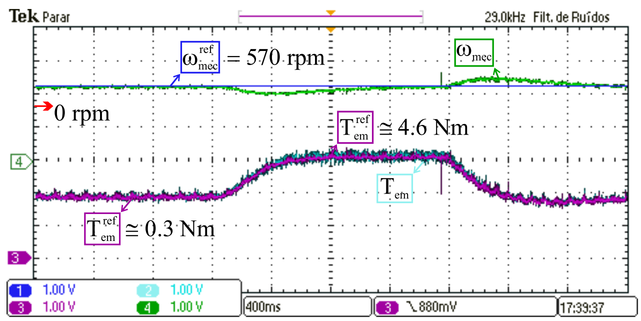

FIGURE 7. **Speed and torque waveforms for dynamic response of the proposed control method under partial load application.**

C. STEADY-STATE BEHAVIOR UNDER PARAMETER VARIATION CONDITIONS AND COMPARISON WITH CLASSICAL FINITE CONTROL SET

In order to verify the robustness of the proposed control method against parameter mismatches, its steady-state performance was analyzed when the parameters of the IM are changed. The IM was kept at constant speed of 850 rpm and the load torque is 3.8 N·m for all tests.

In the first experiment, the stator resistance value, R_s, was changed multiplying it by $(1 + \sigma_{R_s})$ for the calculation of the reference voltage, $\vec{v}_{ff}(k)$, in the proposal. Additionally, the variation σ_R is virtually inserted in the control algorithm [28] to allow a comparison between the strategies.

The rotor speed response for the proposal is shown in Fig. 8 (a). In Figs. 8 (b) and (c) was ploted the behavior of the stator current components, $i_{\alpha s}$ and $i_{\beta s}$, and the vector magnitude, $|\vec{i}_{s\alpha\beta}|$, is presented in Fig. 8(d). The values of σ_{R_s} were changed in regular steps along time and they can be seen in Fig. 8 (e).

Next, R_s was changed dividing it by $(1 + \delta_{R_s})$ for the calculation of the reference voltage, maintaining the same conditions from the previous test. The experimental results

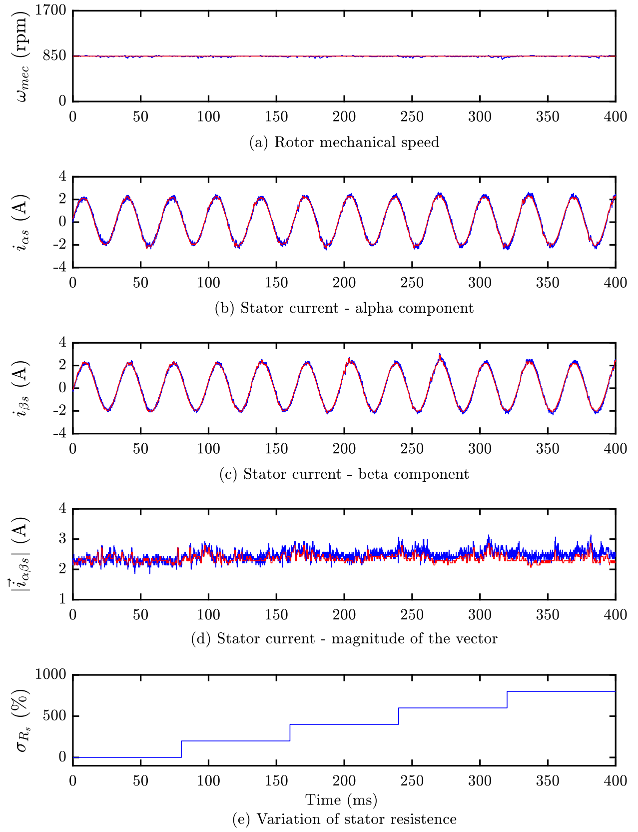

FIGURE 8. Steady-state response of the proposed control under partial load and variations when R_s is multiplied by $(1 + \sigma_{R_S})$. The measured signals are shown in blue and the references in red.

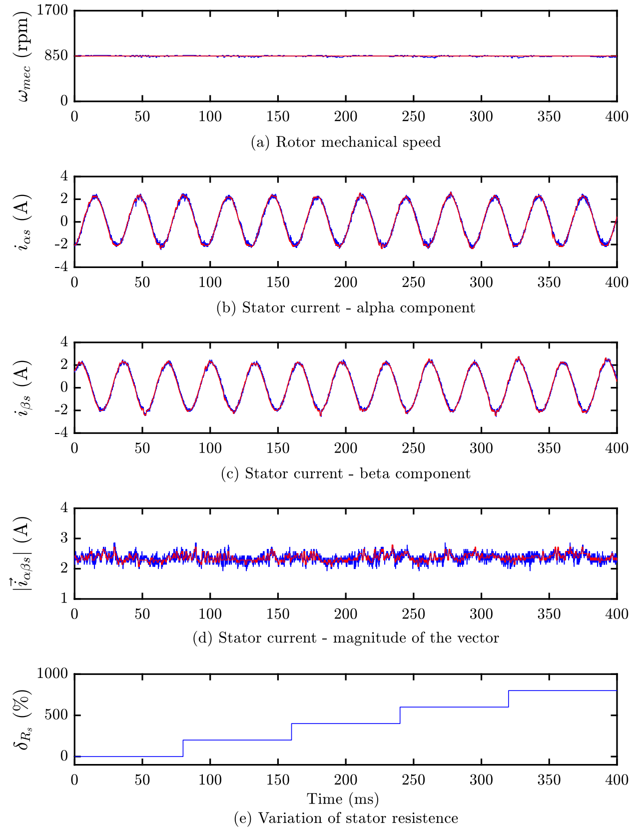

FIGURE 9. Steady-state response of the proposed control under partial load and variations when R_s is divided by $(1 + \sigma_{R_S})$. The measured signals are shown in blue and the references in red.

TABLE 2. MAE, RMSE, MRE, and THD values for the stator current components when R_s is multiplied by $(1 + \sigma_{R_S})$.

Proposed Robust Finite Control Set Current Control					
	σ_{R_s}	$\lvert\vec{i}_{\alpha\beta s}\rvert$	$i_{\alpha s}$	$i_{\beta s}$	ω_{mec}
MAE	0%	0.07 A	0.11 A	0.1 A	5.2 rpm
RMSE		0.09 A	0.14 A	0.12 A	9.7 rpm
MRE		2.9%	-	-	0.6%
THD		-	11.9%	10.7%	-
MAE	800%	0.21 A	0.14 A	0.12 A	5.7 rpm
RMSE		0.22 A	0.17 A	0.15 A	9.7 rpm
MRE		3.7%	-	-	0.7%
THD		-	8.1%	6.1%	-

TABLE 3. MAE, RMSE, MRE, and THD values for the stator current components when R_s is divided by $(1 + \delta_{R_S})$.

Proposed Robust Finite Control Set Current Control					
	δ_{R_s}	$\lvert\vec{i}_{\alpha\beta s}\rvert$	$i_{\alpha s}$	$i_{\beta s}$	ω_{mec}
MAE	0%	0.07 A	0.11 A	0.1 A	6.4 rpm
RMSE		0.09 A	0.14 A	0.12 A	9.3 rpm
MRE		3%	-	-	0.8%
THD		-	8.5%	13.8%	-
MAE	800%	0.07 A	0.11 A	0.1 A	7.3 rpm
RMSE		0.09 A	0.14 A	0.12 A	11.7 rpm
MRE		2.8%	-	-	0.8%
THD		-	9.4%	8.9%	-

are presented in Figs.9(a), (b), (c), (d), and (e), for rotor speed, $i_{\alpha s}$, $i_{\beta s}$, $|\vec{i}_{s\alpha\beta}|$ σ_{R_s}, respectively.

The variation of R_s values did not affect the performance of the controller significantly as it can be seen in the data presented in the Tables 2 and 3. Under the maximum variation of 800%, the MAE and the RMSE did not ultrapass $0.14A$. Only in $|\vec{i}_{\alpha\beta s}|$ an increase of MRE from 2.9% to 3.7% could be seen.

The impact of the variation of R_r values presented in Figs. 10(a), (b), (c), (d), (e) when R_r is multiplied by $(1+\sigma_{R_r})$ for rotor speed, $i_{\alpha s}$, $i_{\beta s}$, $|\vec{i}_{s\alpha\beta}|$ σ_{R_r}, respectively. And Figs.11(a), (b), (c), (d), and (e) when R_r is divided by $(1+\sigma_{R_r})$ for rotor speed, $i_{\alpha s}$, $i_{\beta s}$, $|\vec{i}_{s\alpha\beta}|$ σ_{R_r}, respectively. Therefore, the data presented in Tables 4 and 5 confirm the absence of variations visualized in the figures. In the same way as the tests presented when variations occur in R_s value.

Other tests were conducted for simultaneous variations in both resistances, and this time the proposed robust finite control set model predictive control was compared to the classical current finite control set [28] with the same rotor field orientation depicted in Fig. 1.

The classical predictive current control [28] was tested under the same conditions described to the proposal. The resistances R_r and R_s were changed multiplying them by $(1 + \sigma_R)$. The signals of speed, current components, current vector magnitude, and imposed variations are presented in

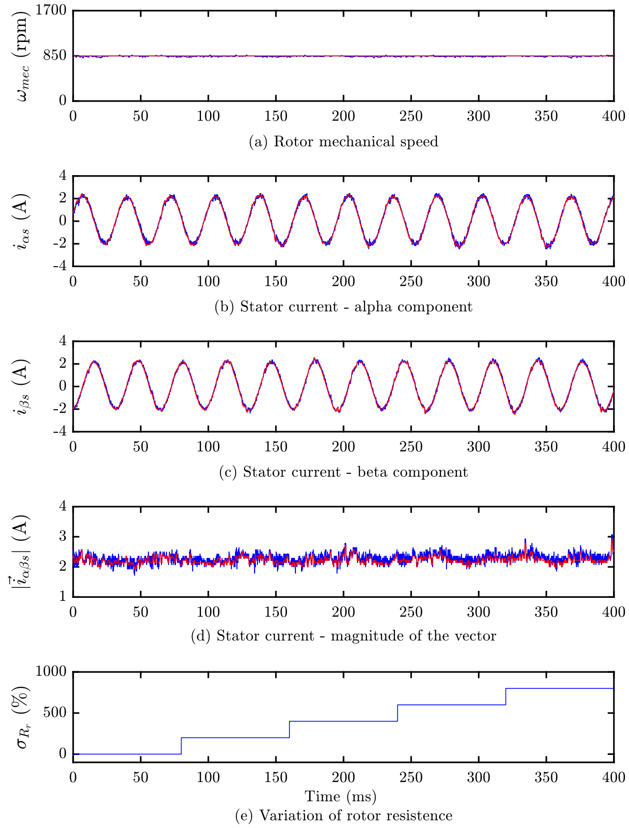

FIGURE 10. Steady-state response of the proposed control under partial load and variations when R_r is multiplied by $(1 + \sigma_{R_r})$. The measured signals are shown in blue and the references in red.

TABLE 4. MAE, RMSE, MRE, and THD values for the stator current components when R_r is multiplied by $(1 + \sigma_{R_r})$.

Proposed Robust Finite Control Set Current Control					
	σ_{R_r}	$\lvert\vec{i}_{\alpha\beta s}\rvert$	$i_{\alpha s}$	$i_{\beta s}$	ω_{mec}
MAE	0%	0.08 A	0.11 A	0.09 A	7.2 rpm
RMSE		0.1 A	0.14 A	0.11 A	12 rpm
MRE		3.4%	-	-	0.9%
THD		-	10.6%	7.3%	-
MAE	800%	0.10 A	0.09 A	0.09 A	6.3 rpm
RMSE		0.13 A	0.12 A	0.11 A	10.6 rpm
MRE		3.7%	-	-	0.8%
THD		-	8.8%	7.1%	-

Figs.12(a), (b), (c), (d), and (e), respectively, for the proposal, and Figs.13(a), (b), (c), (d), and (e), respectively, for the classical current finite control.

Both strategies were able to maintain the rotor speed next to 850 rpm. However, the proposed robust finite control set demonstrates a superior performance when it is considered the MAE, RMSE, MRE, and THD values for the stator current components, as presented in Table 6, considering the max (800%) variation.

Keeping the same boundary conditions, R_r and R_s were also changed dividing them by $(1 + \delta_R)$. The speed, the stator current components, the current vector magnitude and the variation δ signals are presented in

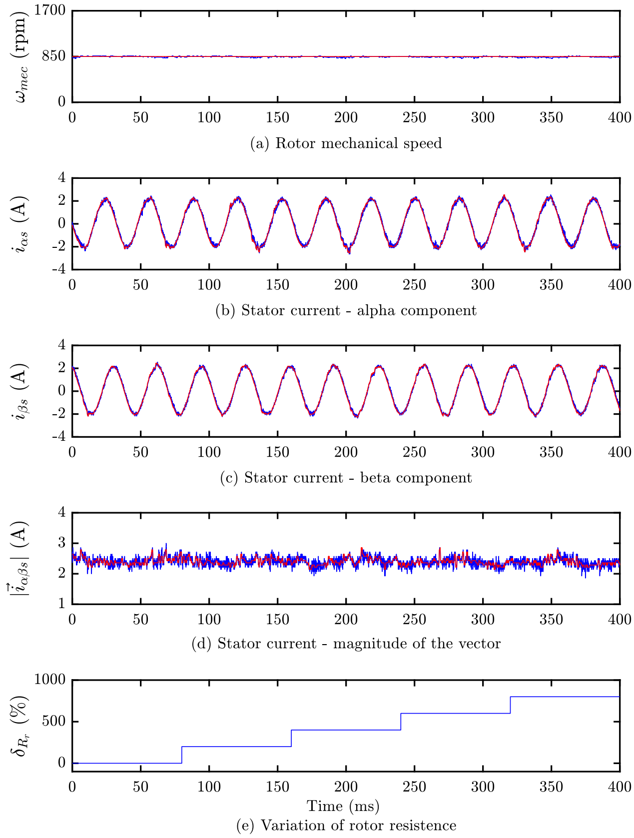

FIGURE 11. Steady-state response of the proposed control under partial load and variations when R_r is multiplied by $(1 + \sigma_{R_r})$. The measured signals are shown in blue and the references in red.

TABLE 5. MAE, RMSE, MRE, and THD values for the stator current components when R_r is divided by $(1 + \delta_{R_r})$.

Proposed Robust Finite Control Set Current Control					
	δ_{R_r}	$\lvert\vec{i}_{\alpha\beta s}\rvert$	$i_{\alpha s}$	$i_{\beta s}$	ω_{mec}
MAE	0%	0.07 A	0.11 A	0.1 A	7.8 rpm
RMSE		0.09 A	0.14 A	0.12 A	11.1 rpm
MRE		2.8%	-	-	0.9%
THD		-	16.8%	13.4%	-
MAE	800%	0.07 A	0.12 A	0.1 A	10.2 rpm
RMSE		0.1 A	0.15 A	0.13 A	13.4 rpm
MRE		3%	-	-	1.2%
THD		-	10.7%	7.5%	-

Figs.14(a), (b), (c), (d), and (e), respectively, for the proposal. The same signals are depicted in Figs. 15(a), (b), (c), (d), and (e), respectively, for the classical predictive current control.

The proposed robust finite control set current controller was able to keep the current elements close to their references under all range of variations but with smaller error ranges when compared to the classical approach. The MAE, RMSE, MRE, and THD values for the stator current components during parameters variations test can be observed in Table 7.

The effect of variation of inductances values was also verified in another test. The most significant impact occurred

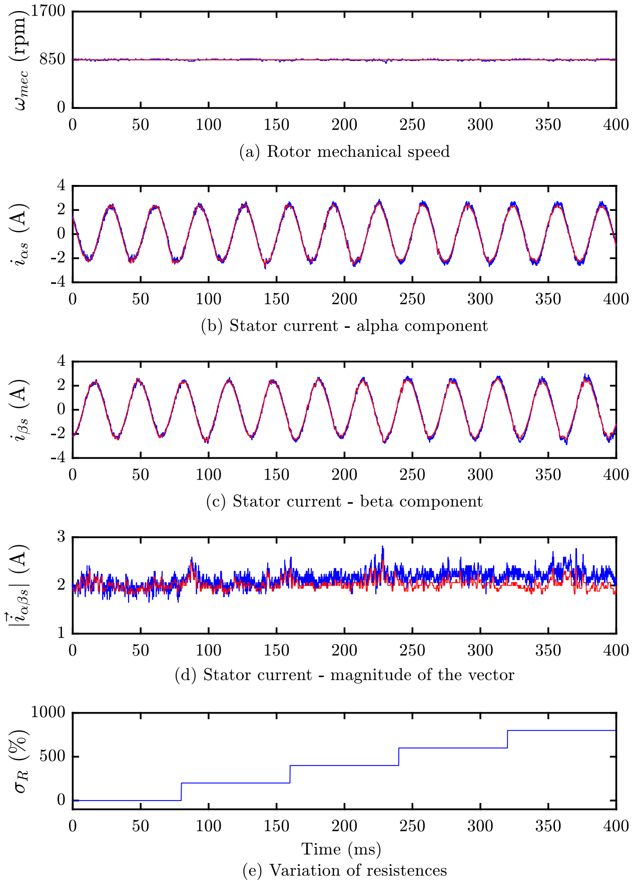

FIGURE 12. **Steady-state response of the proposed control under partial load and variations of $(1+\sigma_R)$ in the rotor and stator resistance values. The measured signals are shown in blue and the references in red.**

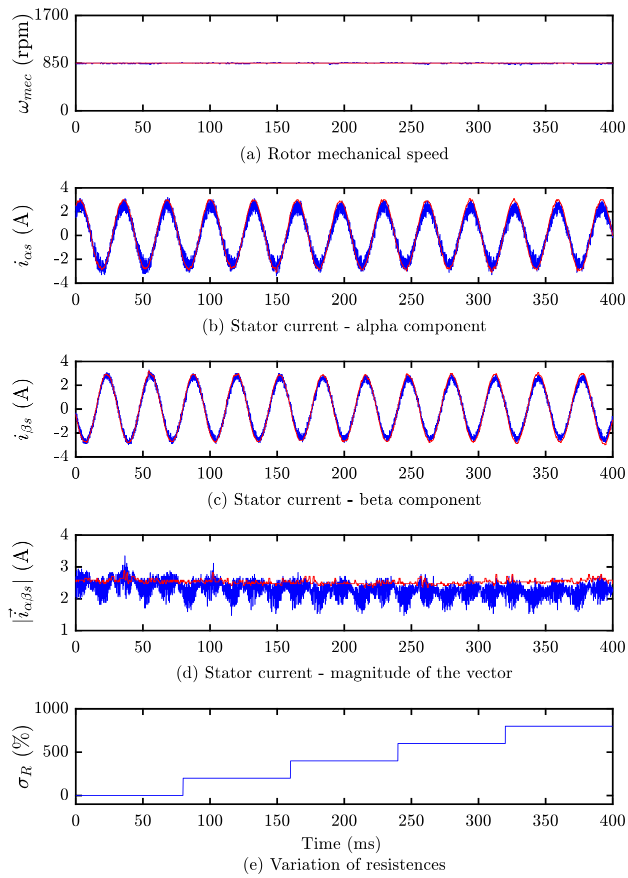

FIGURE 13. **Steady-state response of the classical predictive current control [28] under partial load and variations of $(1+\sigma_R)$ in the rotor and stator resistance values. The measured signals are shown in blue and the references in red.**

TABLE 6. **MAE, RMSE, MRE, and THD values for the stator current components when R_r and R_s are multiplied by $(1+\sigma_R)$.**

Proposed Robust Finite Control Set Current Control					
	σ_R	$\lvert\vec{i}_{\alpha\beta s}\rvert$	$i_{\alpha s}$	$i_{\beta s}$	ω_{mec}
MAE	0%	0.06 A	0.13 A	0.1 A	5.1 rpm
RMSE		0.08 A	0.16 A	0.13 A	7.9 rpm
MRE		1.7%	-	-	0.6%
THD		-	9.4%	7.8%	-
MAE	800%	0.24 A	0.18 A	0.18 A	6.6 rpm
RMSE		0.25 A	0.21 A	0.21 A	9.3 rpm
MRE		4%	-	-	0.8%
THD		-	8%	10.1%	-
Classical predictive current control [28]					
MAE	0%	0.19 A	0.37 A	0.17 A	4.6 rpm
RMSE		0.25 A	0.46 A	0.21 A	7.6 rpm
MRE		7.6%	-	-	0.6%
THD		-	20.3%	13.9%	-
MAE	800%	0.37 A	0.47 A	0.31 A	8.6 rpm
RMSE		0.42 A	0.58 A	0.36 A	11.3 rpm
MRE		8.4%	-	-	1%
THD		-	22.1%	13.3%	-

TABLE 7. **MAE, RMSE, MRE, and THD values for the stator current components when R_r and R_s are divided by $(1+\delta_R)$.**

Proposed Robust Finite Control Set Current Control					
	δ_R	$\lvert\vec{i}_{\alpha\beta s}\rvert$	$i_{\alpha s}$	$i_{\beta s}$	ω_{mec}
MAE	0%	0.05 A	0.12 A	0.1 A	5.8 rpm
RMSE		0.07A	0.16 A	0.13 A	9.8 rpm
MRE		2.6%	-	-	0.7%
THD		-	15.1%	9.5%	-
MAE	800%	0.06 A	0.13 A	0.11 A	5.9 rpm
RMSE		0.08 A	0.17 A	0.14 A	9.6 rpm
MRE		2.8%	-	-	0.7%
THD		-	9.1%	7.6%	-
Classical predictive current control [28]					
MAE	0%	0.19 A	0.35 A	0.17 A	3.6 rpm
RMSE		0.25 A	0.44 A	0.21 A	7.3 rpm
MRE		8.2%	-	-	0.4%
THD		-	23%	11.7%	-
MAE	800%	0.18 A	0.35 A	0.16 A	2 rpm
RMSE		0.24 A	0.43 A	0.21 A	5 rpm
MRE		7.8%	-	-	0.2%
THD		-	21.4%	10.6%	-

when the mutual and leakage inductances were divided by $(1+\delta_L)$ as presented in Figs. 16(a), (b), (c), (d), (e), respectively, for the proposal and 17(a), (b), (c), (d), and (e), respectively, for the classical predictive current control.

The classical predictive current control [28] demonstrated poor responses for $i_{\alpha s}$ and $|\vec{i}_{\alpha\beta s}|$ when δ_L increases. According to the Table 8, the RMSEs of $i_{\alpha s}$ for the classical predictive current control were more than two times greater than

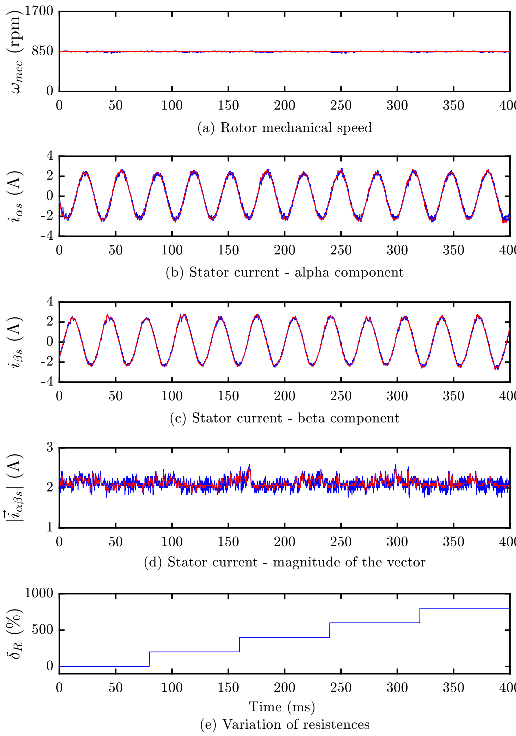

FIGURE 14. Steady-state response of the proposed control under partial load and variations of $(1 + \delta_R)$ in the rotor and stator resistance values. The measured signals are shown in blue and the references in red.

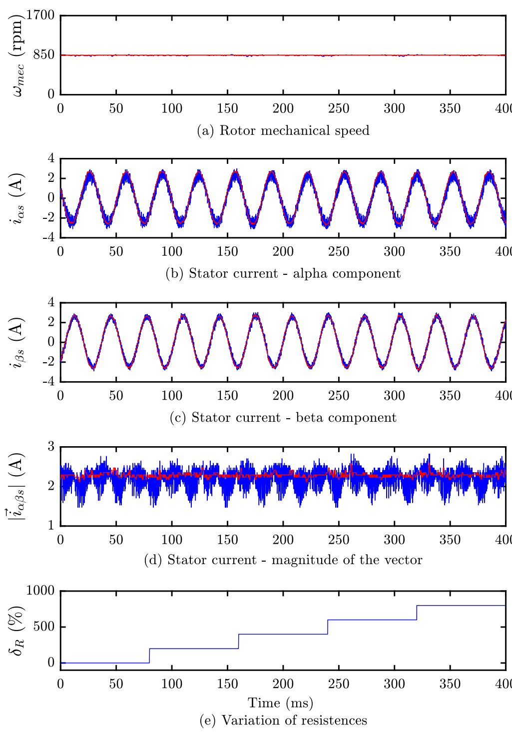

FIGURE 15. Steady-state response of the classical predictive current control [28] under partial load and variations of $(1 + \delta_R)$ in the rotor and stator resistance values. The measured signals are shown in blue and the references in red.

those values registered for the proposed robust predictive current control. The instability recorded in the experimental

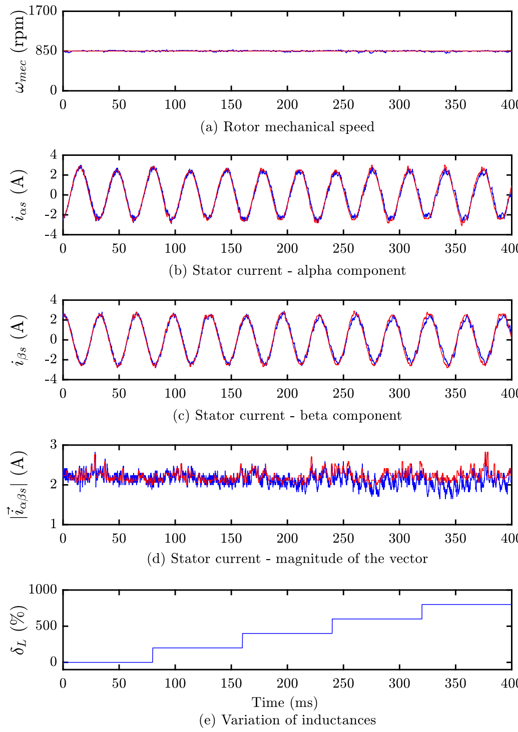

FIGURE 16. Steady-state response of the proposed control under partial load and variations of $(1 + \delta_L)$ in the inductance values. The measured signals are shown in blue and the references in red.

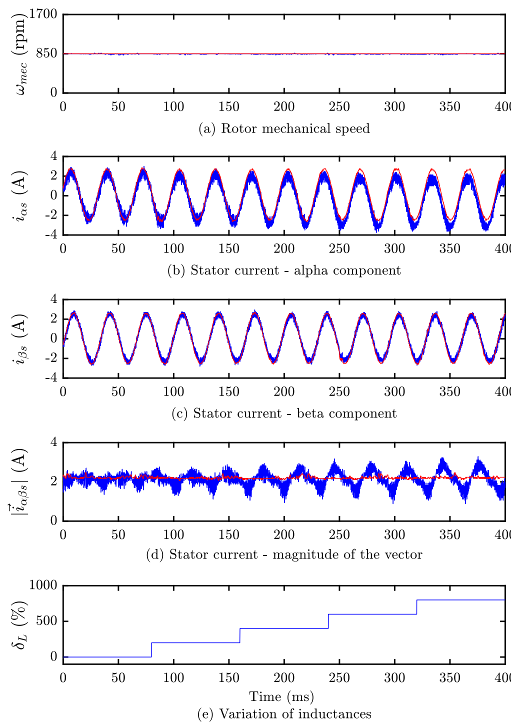

FIGURE 17. Steady-state response of the predictive current control under partial load and variations of $(1 + \delta_L)$ in the inductance values. The measured signals are shown in blue and the references in red.

values of $|\vec{i}_{\alpha\beta s}|$ leads to MRE $=$ 18.4% for the classical controller, while the proposal presented MRE $=$ 4.4% in case $\delta_L = 800\%$.

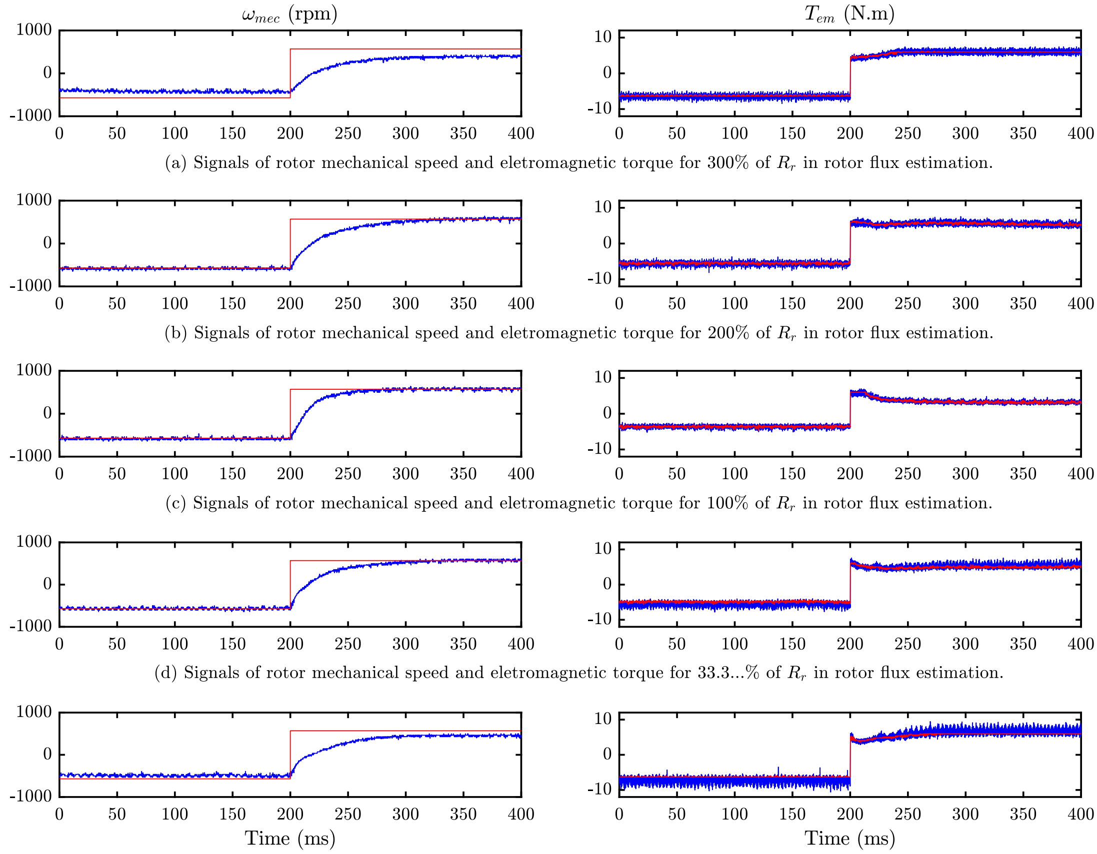

(a) Signals of rotor mechanical speed and eletromagnetic torque for 300% of R_r in rotor flux estimation.

(b) Signals of rotor mechanical speed and eletromagnetic torque for 200% of R_r in rotor flux estimation.

(c) Signals of rotor mechanical speed and eletromagnetic torque for 100% of R_r in rotor flux estimation.

(d) Signals of rotor mechanical speed and eletromagnetic torque for 33.3...% of R_r in rotor flux estimation.

(e) Signals of rotor mechanical speed and eletromagnetic torque for 20% of R_r in rotor flux estimation.

FIGURE 18. **Step response of the proposed control under partial load and rotor resistance variation values applied in rotor flux angle estimation. The measured signals are shown in blue and the references in red.**

TABLE 8. **MAE, RMSE, MRE, and THD values for the stator current components when mutual and leakage inductances are divided by $(1 + \delta_R)$.**

Proposed Robust Finite Control Set Current Control					
	δ_L	$\lvert\vec{i}_{\alpha\beta s}\rvert$	$i_{\alpha s}$	$i_{\beta s}$	ω_{mec}
MAE	0%	0.05 A	0.12 A	0.12 A	7.3 rpm
RMSE		0.08 A	0.16 A	0.15 A	11 rpm
MRE		2.5%	-	-	0.9%
THD		-	8.6%	8.5%	-
MAE	800%	0.12 A	0.24 A	0.12 A	8.9 rpm
RMSE		0.17 A	0.3 A	0.16 A	13.4 rpm
MRE		4.4%	-	-	1%
THD		-	13.7%	14%	-
Classical predictive current control [28]					
MAE	0%	0.19 A	0.3 A	0.17 A	3 rpm
RMSE		0.26 A	0.38 A	0.22 A	7 rpm
MRE		8.5%	-	-	0.4%
THD		-	22.3%	12.6%	-
MAE	800%	0.41 A	0.61 A	0.25 A	5.3 rpm
RMSE		0.49 A	0.67 A	0.3 A	8.2 rpm
MRE		18.4%	-	-	0.6%
THD		-	19.5%	13.4%	-

D. IMPACTS OF PARAMETERS VARIATION OVER FLUX ESTIMATION

Due to the importance of the rotor flux angle estimation in the proposed control algorithm, its sensitivity to variations in the parameter R_r was also investigated. These alterations can affect the dynamic response of the control, which could be evaluated through the execution of step response tests for rotor speed as depicted in Figs. 18(a), (b), (c), (d), and (e), respectively. The speed was varied from -570 rpm to 570 rpm keeping 6 N·m as maximum torque reference generated by the speed PI control where the gains are 0.1 for the proportional gain and 0.3 for the integral gain. The value of R_r was changed only for the calculation of $\theta(k)$ depicted in Fig. 1. It can be observed that the torque reaches the references. However, there is a speed error of more than 5% in Fig. 18(a). It can be corrected by considering other values of the PI gains.

Although outside the scope of this work, there are new observer alternatives for estimating rotor flux as presented in [29], [30], and [31]. So that, they can be incorporated into the proposed control, improving its performance.

IV. CONCLUSION

This paper proposes a robust finite control set model predictive current control for IM using IFOC in stationary reference frame. The proposal calculates the applied stator voltage vector as a sum of two voltages elements: one employs the classical MPC and another one considering the deadbeat approach to compensate parameter mismatch. Hence, the stator voltage vector is selected using the minimized cost function.

The proposal demonstrated strong robustness considering the variations in the IM resistance values. Even variations of 800% of the nominal values did not compromise the steady-state performance, indicating potential for applications that require stability in the control of IM. The experimental results endorse dynamic-state and steady-state performances for the proposed control and its superiority over classical predictive current control. The impact of parametric mismatches on the rotor flux orientation was also analyzed and it can be observed that the strategy works satisfactorily even when the rotor resistance varies up to 300%.

REFERENCES

[1] W. Qinglong, Y. Changzhou, and Y. Shuying, ''Indirect field oriented control technology for asynchronous motor of electric vehicle,'' in *Proc. IEEE Int. Conf. Power, Intell. Comput. Syst. (ICPICS)*, Jul. 2020, pp. 673–677.

[2] G. S. Buja and M. P. Kazmierkowski, ''Direct torque control of PWM inverter-fed AC motors—A survey,'' *IEEE Trans. Ind. Electron.*, vol. 51, no. 4, pp. 744–757, Aug. 2004.

[3] M. P. Kazmierkowski, L. G. Franquelo, J. Rodriguez, M. A. Perez, and J. I. Leon, ''High-performance motor drives,'' *IEEE Ind. Electron. Mag.*, vol. 5, no. 3, pp. 6–26, Sep. 2011.

[4] M. Nagataki, K. Kondo, O. Yamazaki, K. Yuki, and Y. Nakazawa, ''Online auto-tuning method in field-orientation-controlled induction motor driving inertial load,'' *IEEE Open J. Ind. Appl.*, vol. 3, pp. 125–140, 2022.

[5] V. Kousalya, R. Rai, and B. Singh, ''Sliding model-based predictive torque control of induction motor for electric vehicle,'' *IEEE Trans. Ind. Appl.*, vol. 58, no. 1, pp. 742–752, Jan./Feb. 2022.

[6] J. Rodriguez, ''Latest advances of model predictive control in electrical drives—Part II: Applications and benchmarking with classical control methods,'' *IEEE Trans. Power Electron.*, vol. 37, no. 5, pp. 5047–5061, May 2022.

[7] M. Khalilzadeh, S. Vaez-Zadeh, J. Rodriguez, and R. Heydari, ''Model-free predictive control of motor drives and power converters: A review,'' *IEEE Access*, vol. 9, pp. 105733–105747, 2021.

[8] J. Rodriguez, M. P. Kazmierkowski, J. R. Espinoza, P. Zanchetta, H. Abu-Rub, H. A. Young, and C. A. Rojas, ''State of the art of finite control set model predictive control in power electronics,'' *IEEE Trans. Ind. Informat.*, vol. 9, no. 2, pp. 1003–1016, May 2013.

[9] S. Vazquez, J. I. Leon, L. G. Franquelo, J. Rodriguez, H. A. Young, A. Marquez, and P. Zanchetta, ''Model predictive control: A review of its applications in power electronics,'' *IEEE Ind. Electron. Mag.*, vol. 8, no. 1, pp. 16–31, Mar. 2014.

[10] Z. Zhang, M. A. Gultekin, and A. M. Bazzi, ''State-space modeling of multi-mode-controlled induction motor drive,'' in *Proc. IEEE Int. Electric Mach. Drives Conf. (IEMDC)*, May 2021, pp. 1–5.

[11] A. J. S. Filho, A. L. de Oliveira, L. L. Rodrigues, E. C. M. Costa, and R. V. Jacomini, ''A robust finite control set applied to the DFIG power control,'' *IEEE J. Emerg. Sel. Topics Power. Electron.*, vol. 6, no. 4, pp. 1692–1698, Dec. 2018.

[12] Z. Zhang, Y. Liu, X. Liang, H. Guo, and X. Zhuang, ''Robust model predictive current control of PMSM based on nonlinear extended state observer,'' *IEEE J. Emerg. Sel. Topics Power Electron.*, early access, Jul. 21, 2022, doi: 10.1109/JESTPE.2022.3192064.

[13] E. R. C. Duque, A. Lunardi, J. S. Solís-Chaves, T. D. S. Paiva, D. A. Fernandes, and A. J. S. Filho, ''Improvement of robustness of MPC adding repetitive behavior for the DFIG current control,'' *Energies*, vol. 15, no. 11, p. 4114, Jun. 2022. [Online]. Available: https://www.mdpi.com/1996-1073/15/11/4114

[14] F. Stinga and D. Popescu, ''Robust model predictive control of an induction motor,'' in *Proc. 18th Int. Conf. Syst. Theory, Control Comput. (ICSTCC)*, Oct. 2014, pp. 381–386.

[15] M. Mousavi, S. A. Davari, V. Nekoukar, C. Garcia, L. He, F. Wang, and J. Rodriguez, ''Predictive torque control of induction motor based on a robust integral sliding mode observer,'' *IEEE Trans. Ind. Electron.*, early access, Apr. 29, 2022, doi: 10.1109/TIE.2022.3169831.

[16] Y. Zhang, X. Wang, B. Zhang, and H. Yang, ''A robust model-free predictive current control of induction motor drives,'' in *Proc. 22nd Int. Conf. Electr. Mach. Syst. (ICEMS)*, Aug. 2019, pp. 1–5.

[17] X. Wang, Y. Zhang, H. Yang, B. Zhang, J. Rodriguez, and C. Garcia, ''A model-free predictive current control of induction motor based on current difference,'' in *Proc. IEEE 9th Int. Power Electron. Motion Control Conf. (IPEMC-ECCE Asia)*, Nov. 2020, pp. 1038–1042.

[18] X. Wang, Y. Zhang, H. Yang, B. Zhang, and J. Rodriguez, ''A robust predictive current control of induction motor drives,'' in *Proc. IEEE Energy Convers. Congr. Expo. (ECCE)*, Oct. 2020, pp. 5136–5140.

[19] Y. Zhang, X. Wang, H. Yang, B. Zhang, and J. Rodriguez, ''Robust predictive current control of induction motors based on linear extended state observer,'' *Chin. J. Electr. Eng.*, vol. 7, no. 1, pp. 94–105, 2021.

[20] J. Wang, F. Wang, G. Wang, S. Li, and L. Yu, ''Generalized proportional integral observer based robust finite control set predictive current control for induction motor systems with time-varying disturbances,'' *IEEE Trans. Ind. Informat.*, vol. 14, no. 9, pp. 4159–4168, Sep. 2018.

[21] X. Wang, Y. Zhang, and H. Yang, ''Enhanced robust deadbeat predictive current control for induction motors,'' in *Proc. IEEE Int. Conf. Predictive Control Electr. Drives Power Electron. (PRECEDE)*, Nov. 2021, pp. 600–604.

[22] B. Wang, Y. Yu, X. Chen, C. Wang, B. Li, and D. Xu, ''Robust predictive current control for induction motor in synchronous rotating frame,'' in *Proc. 8th IET Int. Conf. Power Electron., Mach. Drives (PEMD)*, 2016, pp. 1–5.

[23] L. Yan, F. Wang, and J. Rodriguez, ''Luenberger prediction model-based robust predictive current control of induction machine drives,'' in *Proc. IEEE 9th Int. Power Electron. Motion Control Conf. (IPEMC-ECCE Asia)*, Nov. 2020, pp. 1006–1010.

[24] A. S. Bazanella and R. Reginatto, ''Robustness margins for indirect field-oriented control of induction motors,'' in *Proc. 37th IEEE Conf. Decis. Control*, vol. 1, Dec. 1998, pp. 1001–1006.

[25] J. Rodriguez and P. Cortes, *Predictive Control of Power Converters and Electrical Drives*, vol. 40. Hoboken, NJ, USA: Wiley, 2012.

[26] A. J. S. Filho, *Model Predictive Control for Doubly-Fed Induction Generators Three-Phase Power Converters*. Amsterdam, The Netherlands: Elsevier, 2022.

[27] S.-M. Yang and C.-H. Lee, ''A deadbeat current controller for field oriented induction motor drives,'' *IEEE Trans. Power Electron.*, vol. 17, no. 5, pp. 772–778, Sep. 2002.

[28] F. Wang, S. Li, X. Mei, W. Xie, J. Rodríguez, and R. M. Kennel, ''Model-based predictive direct control strategies for electrical drives: An experimental evaluation of PTC and PCC methods,'' *IEEE Trans. Ind. Informat.*, vol. 11, no. 3, pp. 671–681, Jun. 2015.

[29] O. Wallscheid and E. F. B. Ngoumtsa, ''Investigation of disturbance observers for model predictive current control in electric drives,'' *IEEE Trans. Power Electron.*, vol. 35, no. 12, pp. 13563–13572, Dec. 2020.

[30] H. Xie, F. Wang, W. Zhang, C. Garcia, J. Rodríguez, and R. Kennel, ''Sliding mode flux observer based predictive field oriented control for induction machine drives,'' in *Proc. IEEE 9th Int. Power Electron. Motion Control Conf. (IPEMC-ECCE Asia)*, Nov. 2020, pp. 3021–3025.

[31] A. Devanshu, M. Singh, and N. Kumar, ''An improved nonlinear flux observer based sensorless FOC IM drive with adaptive predictive current control,'' *IEEE Trans. Power Electron.*, vol. 35, no. 1, pp. 652–666, Jan. 2020.

THIAGO BALDIM DOS SANTOS received the bachelor's degree in energy engineering from the Maua Institute of Technology, in 2019. He is currently pursuing the Ph.D. degree in energy with the Federal University of ABC. His research interests include electrical systems and power electronics applied to electric machine drives and electric vehicles.

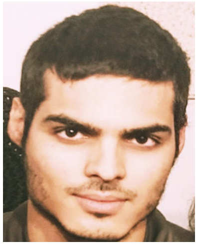

IGOR OLIANI received the bachelor's degree in science and technology from the Federal University of ABC, in 2019, where he is currently pursuing the master's degree in energy engineering and electrical engineering. His research interests include electrical systems and power electronics applied to electric motor drives and electric vehicles.

RAFAEL FIGUEIREDO received the bachelor's degrees in science and technology and automation and in instrumentation and robotics engineering from the Federal University of ABC (UFABC), in 2018 and 2022, respectively, where he is currently pursuing the bachelor's degree in computer science and the master's degree in electrical engineering. He participates with the Power Electronics and Smart Grid Laboratory (LEPS), UFABC. His research interests include power electronics, motor drives, electrification, and renewable energies.

DANIEL ALBIEIRO is graduated from the Faculty of Agricultural Engineering, State University of Campinas (UNICAMP), in 2001, and received the degree in physics and the master's and Ph.D. degrees in agricultural engineering from UNICAMP, in 1996, 2005, and 2009, respectively. He is currently a Professor of agricultural machine design and robotics with the Faculty of Agricultural Engineering (FEAGRI), UNICAMP, and an Extension Coordinator of FEAGRI/UNICAMP. He is experienced in agricultural engineering, with emphasis on soil dynamics, design and evaluation of agricultural machinery, agroecological machinery, equipment for family farming, optics applied to agricultural engineering, rural buildings with alternative material, physical and mechanical properties of biological material, agricultural aviation, quality management in agriculture, energy in agriculture (biomass and wind), and robotics in agriculture.

ADEMIR PELIZARI received the master's and Ph.D. degrees, in 2009 and 2015, respectively. He is currently an Electrical Engineer Graduated with the University of Mogi das Cruzes (UMC), São Paulo, Brazil, in 2002. He is also working as an Adjunct Professor with the Federal University of ABC (UFABC). His research interests include electromechanical devices and electrical machines.

ALFEU J. SGUAREZI FILHO (Senior Member, IEEE) received the master's and Ph.D. degrees in electrical engineering from the Faculty of Electrical and Computer Engineering, University of Campinas (UNICAMP), in 2007 and 2010, respectively. He is currently an Associate Professor with the Federal University of ABC (UFABC). He is the author of several articles published in national and international scientific journals and book chapters. His research interests include electrical machines, machine drives, electric vehicles, power electronics, wind, and photovoltaic energies.